HHS Public Access

Author manuscript

Cell Rep. Author manuscript; available in PMC 2024 December 13.

Published in final edited form as:

Cell Rep. 2024 November 26; 43(11): 114898. doi:10.1016/j.celrep.2024.114898.

Hypothalamic regulation of hippocampal CA1 interneurons by the supramammillary nucleus

Yu-Qiu Jiang[1], **Daniel K. Lee**[1], **Wanyi Guo**[1], **Minghua Li**[1], **Qian Sun**[1,2,*]

[1]Department of Neurosciences, School of Medicine, Case Western Reserve University, 10900 Euclid Avenue, Cleveland, OH 44106, USA

[2]Lead contact

SUMMARY

The hypothalamic supramammillary nucleus (SuM) projects heavily to the hippocampus to regulate hippocampal activity and plasticity. Although the projections from the SuM to the dentate gyrus (DG) and CA2 have been extensively studied, whether the SuM projects to CA1, the main hippocampal output region, is unclear. Here, we report a glutamatergic pathway from the SuM that selectively excites CA1 interneurons in the border between the stratum radiatum (SR) and the stratum lacunosum-moleculare (SLM). We find that the SuM projects selectively to a narrow band in the CA1 SR/SLM and monosynaptically excites SR/SLM interneurons, including vasoactive intestinal peptide-expressing (VIP^+) and neuron-derived neurotrophic factor-expressing ($NDNF^+$) cells, but completely avoids making monosynaptic contacts with CA1 pyramidal neurons (PNs) or parvalbumin-expressing (PV^+) or somatostatin-expressing (SOM^+) cells. Moreover, SuM activation drives spikes in most SR/SLM interneurons to suppress CA1 PN excitability. Taken together, our findings reveal that the SuM can directly regulate hippocampal output region CA1, bypassing CA2, CA3, and the DG.

Graphical Abstract

[*]**Correspondence:** qxs111@case.edu.

AUTHOR CONTRIBUTIONS

Q.S. conceived and supervised the project. Y.-Q.J. and Q.S. designed the research and wrote the manuscript. Y.-Q.J., D.K.L., W.G., M.L., and Q.S. performed the experiments and analyzed the data.

RESOURCE AVAILABILITY

Lead contact

Requests for further information and resources and reagents should be directed to the lead contact, Qian Sun (qxs111@case.edu).

Materials availability

The materials used in this study are all publicly available in the academic or commercial sources.

Data and code availability

- The data reported in this study will be shared from the lead contact upon request.
- This paper does not report original code.
- Any additional information required to reanalyze the data reported in this paper is available from the lead contact upon request.

DECLARATION OF INTERESTS

The authors declare no competing interests.

SUPPLEMENTAL INFORMATION

Supplemental information can be found online at https://doi.org/10.1016/j.celrep.2024.114898.

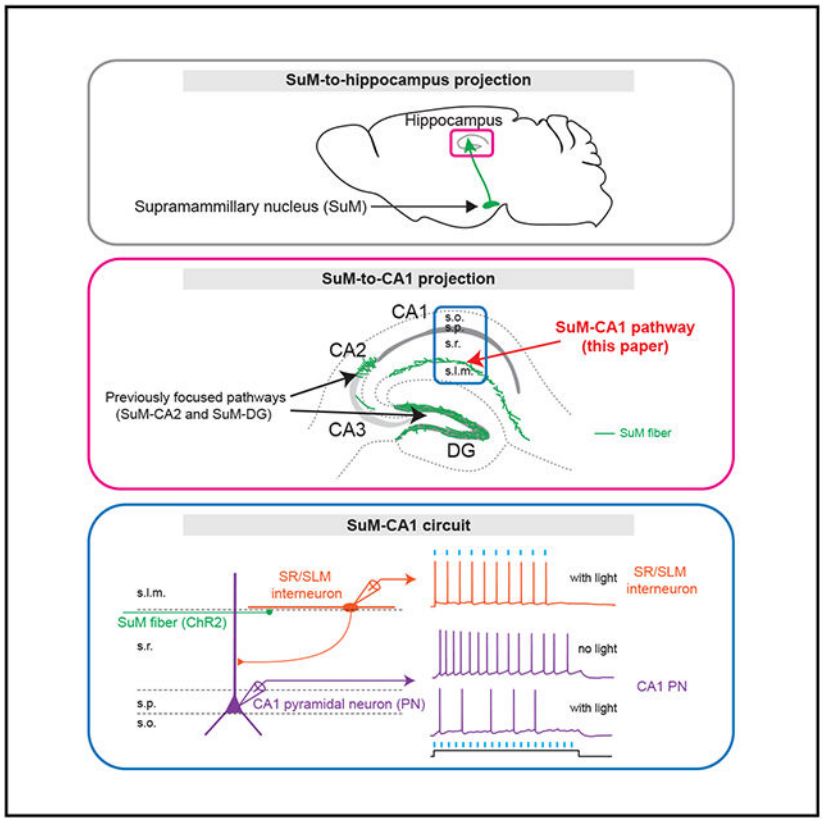

In brief

Jiang et al. report a glutamatergic pathway from the hypothalamic supramammillary nucleus (SuM) that selectively excites CA1 interneurons in the stratum radiatum/stratum lacunosum-moleculare border and completely avoids CA1 pyramidal neurons and parvalbumin- or somatostatin-expressing cells. This study demonstrates that the SuM can directly regulate CA1, bypassing CA2, CA3, and the dentate gyrus.

INTRODUCTION

The supramammillary nucleus (SuM) is a small region in the hypothalamus that participates in various behaviors, including learning and memory, reward, arousal, and social behavior.[1-4] The SuM is known to send long-range projections to the hippocampus and plays an important role in regulating hippocampal activity, plasticity, and several hippocampal-dependent behaviors, such as spatial memory, social behavior, locomotion, and theta oscillations.[5-21] Over the past decade, most studies on SuM-hippocampus projections have focused on its two pathways to the dentate gyrus (DG) and CA2, respectively.[7-9,11-14,16,21-26] For example, recent studies have shown that the SuM-DG projection regulates adult neurogenesis in the DG and participates in spatial learning,[6,7,11,14] whereas the SuM-CA2 projection is involved in social behavior.[8,12] In comparison, the projection from the SuM to other hippocampal regions, including CA1 and CA3, remains largely unexplored. This neglect is perhaps not surprising, given the dense SuM fibers

concentrated in CA2 and the DG.[12,19,22,24,27] We have previously demonstrated that the sparse innervation of the SuM in CA3 can robustly excite CA3 interneurons, including parvalbumin-expressing (PV^+) cells, to provide feedforward inhibition onto nearly all CA3 pyramidal neurons (PNs), underscoring the functional importance of sparse innervation.[5] Yet, whether the SuM projects to CA1, the primary hippocampal output region, is unclear. In this study, we fill this critical gap in knowledge by investigating the anatomic and functional connectivity between the SuM and CA1.

Area CA1 is the last stage of the hippocampal trisynaptic pathway and is essential for memory formation.[28] CA1 activity is regulated by a highly diverse group of interneurons that are distributed across different layers, including a group of less-studied interneurons in the border between the stratum radiatum (SR) and the stratum lacunosum-moleculare (SLM).[29-34] Although CA1 is known to receive long-range glutamatergic inputs from several subcortical regions,[35] detailed functional analyses of postsynaptic CA1 PNs versus interneurons targeted by subcortical inputs remain scarce. Given the functional heterogeneity of CA1 interneurons,[29,30,34] it will be valuable to identify postsynaptic cell types targeted by subcortical inputs.

In this study, we addressed the above questions by focusing on a pathway from the SuM to CA1. We demonstrate that, in contrast with its projections to other hippocampal regions, the SuM projects selectively to a distinct narrow band in the CA1 SR/SLM border, where a diverse group of interneurons is located.[29,31] We further show that SuM inputs powerfully excite CA1 SR/SLM interneurons, including vasoactive intestinal peptide-expressing (VIP^+) and neuron-derived neurotrophic factor-expressing ($NDNF^+$) cells, but completely avoid making monosynaptic connections with CA1 PNs, PV^+ cells, or somatostatin-expressing (SOM^+) cells. Our results demonstrate that the SuM can directly and powerfully regulate CA1 activity by exciting a selective group of CA1 interneurons, bypassing CA2, CA3, and the DG. Thus, our findings, together with the previous studies,[5-9,11-13,21] demonstrate that the SuM can directly regulate all four hippocampal subregions. But the mode of how the SuM regulates downstream targets varies substantially, depending on the postsynaptic targets in the hippocampus. Moreover, this study, along with our recent work on the SuM-CA3 projection,[5] highlights the significance and complexity of the powerful regulation of downstream targets by sparse but selective innervation onto interneurons. Finally, we argue that the selective excitation of interneurons in CA1 and CA3 by the SuM should be taken into consideration in view of the functions of the SuM-hippocampus circuit.[1]

RESULTS

Anatomic evidence of SuM-CA1 projection

Previous studies,[7-13,16,21,22,27] including ours,[5] have identified the direct anatomic and functional connections between the SuM and CA2, CA3, or the DG. However, whether the SuM projects to and directly regulates area CA1 is unknown. To address this, we bilaterally injected an adeno-associated virus (AAV), AAV-Syn-ChannelRhodopsin2 (ChR2)-EYFP, into the SuM and, after 2 weeks, examined the expression pattern of ChR2-$EYFP^+$ fibers in the hippocampus (Figures 1A and 1B). As expected, we observed dense expression of ChR2-$EYFP^+$ fibers in CA2 and the DG (Figures 1C and 1E). Surprisingly, we also

observed the expression of ChR2-EYFP$^+$ fibers in CA1 (Figures 1C-1E), which has not been reported previously. Interestingly, a close inspection showed that the expression pattern of the SuM fibers in CA1 was distinct from that in CA2 or the DG (Figures 1C-1E). In CA2 and the DG, the dense ChR2-EYFP$^+$ fibers were predominantly observed in either the CA2 stratum pyramidale (SP) or the DG granule cell layer (GCL) (Figures 1C and 1E), consistent with previous studies.[5,12,22,27] In stark contrast, the ChR2-EYFP$^+$ fibers in CA1 were largely restricted to a narrow band in the SR/SLM border along the CA1 transverse axis and were very sparse in all other layers (Figures 1C-1E). An analysis of fluorescence intensity along the CA1 radial axis revealed a sharp peak of EYFP fluorescence intensity in the SR/SLM border (Figure 1D).

Next, we used AAVretro-Cre to target a Cre-dependent AAV-DIO-ChR2-EYFP into CA1-projecting SuM neurons (Figures 1F-1I).[36] We first unilaterally injected an AAV retrograde carrying Cre recombinase (AAVretro-Cre-mCherry) into dorsal CA1, which would be retrogradely expressed in SuM neurons that project to CA1 (Figures 1F, 1G, and S1). We injected a second Cre-dependent AAV-DIO-ChR2-EYFP into the SuM 2 weeks later, resulting in the expression of ChR2-EYFP in SuM neurons (ChR2-EYFP$^+$ cells, 39.3 ± 6.7 per section; n = 4 sections/3 mice) (Figures 1F, 1G, and S1). Consistent with the general tracing of SuM neurons above (Figures 1A-1E), we detected the abundant expression of ChR2-EYFP$^+$ fibers in the CA1 SR/SLM border along the transverse axis, with very sparse expression in other CA1 layers (Figures 1H and 1I). Taken together, the neural tracing results provide strong anatomic evidence that the SuM preferentially projects to the SR/SLM border in CA1.

Selective excitation of CA1 SR/SLM interneurons by the SuM

Given the presence of a large number of interneurons along the CA1 SR/SLM border,[29,31,32] we hypothesized that the relatively restricted expression of SuM fibers in the SR/SLM border indicated that SuM inputs may selectively target GABAergic neurons in CA1. To test this, we injected AAV-Syn-ChR2-EYFP bilaterally into the SuM and prepared acute dorsal transverse hippocampal slices 3–5 weeks later for *ex vivo* whole-cell recordings in SR/SLM interneurons (Figures 2A-2C). As expected, the electrophysiological properties of SR/SLM interneurons, such as resting membrane potential, input resistance, and action potential (AP) properties, differ significantly from CA1 PNs (Figure S2). Remarkably, light pulses evoked large excitatory synaptic responses in a majority of cells recorded in the CA1 SR/SLM border (77.8%, 35/45 cells; excitatory postsynaptic current [EPSC] = −153.6 ± 25.5 pA, n = 35 cells; Figures 2D and 2L). Light-evoked EPSCs were completely blocked by bath application of 6,7-dinitroquinoxaline-2,3-dione (DNQX, 20 μM) and DL-2-Amino-5-phosphonovaleric acid (APV, 50 μM), the AMPAR and NMDAR antagonists, indicating that the SuM-CA1 interneuron synapses are glutamatergic (Figures 2E and 2F). In addition, bath application of tetrodotoxin (TTX; 1 μM) completely abolished light-evoked EPSCs, which reappeared after the addition of 4-aminopyridine (4-AP; 1 mM) (repeated in three cells) (Figure 2G), confirming monosynaptic connections.

Because previous studies found that the SuM-DG synapses are dual glutamatergic and GABAergic,[11,13,23] we asked whether SuM terminals in CA1 SR/SLM also release GABA.

We performed voltage-clamp recording using Cs-based intracellular solution to measure light-evoked inhibitory postsynaptic currents (IPSCs) in SR/SLM interneurons by holding the membrane potential at 0 mV. Light-evoked IPSCs were detected in only a fraction of SR/SLM interneurons (38.1%, $n = 8/21$ cells/4 mice). Importantly, bath application of DNQX/APV abolished light-evoked IPSCs (Figures 2H and 2I, DNQX/APV = 4.83 ± 1.2% of baseline, $n = 6$ cells/3 mice, $p = 7.1 \times 10^{-9}$, paired t test), arguing against monosynaptic inhibitory connections between SuM and CA1 SR/SLM interneurons. Moreover, the onset of light-evoked IPSCs was significantly longer than that of EPSCs (Figure 2J, EPSCs, 1.13 ± 0.07 ms, $n = 35$ cells/9 mice; IPSCs, 3.63 ± 0.37 ms, $n = 8$ cells/3 mice, $p = 7.1 \times 10^{-14}$, unpaired t test), suggesting the inhibitory responses in SR/SLM interneurons are disynaptic feedforward inhibition. Finally, a train of 10–20 Hz light stimulation reliably elicited APs in more than half of SR/SLM cells tested (57.8%, 26/45 cells; Figures 2K and 2M). Taking these results together, we conclude that SuM inputs make powerful pure glutamatergic monosynaptic connections and can drive suprathreshold APs in most of CA1 SR/SLM interneurons.

The SuM excites but fails to elicit spikes in CA1 NDNF$^+$ cells

The interneurons in the CA1 SR/SLM border are highly diverse.[29,31,32] Next, we sought to explore the cell identity of postsynaptic targets of the SuM. We first investigated its connections with neurogliaform cells, a major subtype of interneurons predominantly residing in the SLM and SR/SLM border.[31,32,37-39] To identify neurogliaform cells during patch-clamp recording, we took advantage of the NDNF-Cre mouse line, which has been used to target neurogliaform cells in CA1 SLM.[40] We generated NDNF-td mice by crossing an NDNF-Cre line with an Ai9 tdTomato reporter line (Figure 3A). AAV-Syn-ChR2-EYFP was bilaterally injected into the SuM in NDNF-td mice (Figures 3B and 3C). Current-clamp recording confirmed that NDNF$^+$ cells in the CA1 SR/SLM displayed electrophysiological features that are consistent with neurogliaform cells, such as relatively hyperpolarized resting potential (−62.4 ± 1.1 mV, $n = 20$ cells), small AP amplitude (65.9 ± 4.0 mV, $n = 20$ cells), and relatively wide AP half-width (0.70 ± 0.02 ms, $n = 20$ cells) (Figures S3D-S3K).[37,41] We found that only half of NDNF$^+$ cells received the excitatory input from the SuM (50%, 10/20 cells) (Figures 3E and 3H). In addition, light-evoked EPSCs in NDNF$^+$ cells were significantly smaller than those in SR/SLM interneurons recorded randomly (Figure 3G, SR/SLM interneurons, −153.58 ± 25.47 pA, $n = 35$ cells; NDNF$^+$ cells, −46.76 ± 11.61 pA, $n = 10$ cells, $p = 0.00043$, unpaired t test). Finally, unlike SR/SLM interneurons recorded randomly, a train of 10–20 Hz light stimulation failed to elicit APs in all NDNF$^+$ cells tested (0%, 0/20 cells) (Figures 3F and 3I). Taken together, we conclude that, although a significant proportion of NDNF$^+$ cells did receive excitatory input from the SuM, the relatively weak excitatory connections were insufficient to drive AP output in NDNF$^+$ cells.

The SuM excites VIP$^+$ cells in CA1

Next, we examined the connectivity between the SuM and a subtype of VIP$^+$ cells–interneuron-specific type 2—that reside near the CA1 SR/SLM (Figure 4).[33,34,42,43] We identified VIP$^+$ cells by crossing a VIP-IRES-Cre line[44] with an Ai9 tdTomato line and recorded and compared VIP$^+$ and VIP$^-$ cells from the same slices (Figures 4A-4D).

Interestingly, we found that an approximately equally high percentage of VIP^+ and VIP^- cells in the SR/SLM border received the light-evoked excitatory responses (Figures 4E and 4F). The connectivity probability was very high and comparable between VIP^+ and VIP^- cells (VIP^+ cells, 90.5%, 19/21 cells; VIP^- cells, 90%, 9/10 cells) (Figure 4I). The amplitude of light-evoked EPSCs in VIP^+ cells was significantly smaller than that in VIP^- cells (VIP^+ cells, −39.93 ± 10.92 pA, n = 19 cells; VIP^- cells, −306.13 ± 104.83 pA, n = 9 cells; p = 0.001, unpaired t test) (Figures 4E and 4F). Notably, a train of 10–20 Hz light stimulation was able to evoke spikes in a majority of both VIP^+ and VIP^- cells (Figures 4H and 4J, VIP^+ cells, 52.4%, 11/21 cells; VIP^- cells, 70%, 7/10 cells). The ability to evoke spikes in a relatively high percentage of VIP^+ cells is likely, in part, due to a high input resistance in VIP^+ cells (Figure 4G, VIP^+ cells, 661.0 ± 52.5 MΩ, n = 20 cells; VIP^- cells, 422.3 ± 65.7 MΩ, n = 10 cells; p = 0.011, unpaired t test). Overall, we conclude that VIP^+ cells received weaker SuM-driven EPSCs than VIP^- cells, but the probabilities of connectivity and firing APs were nearly comparable between VIP^+ and VIP^- cells.

The SuM avoids making monosynaptic connections with PV^+ or SOM^+ cells in CA1

We and others have previously reported that in CA2 and CA3, SuM inputs strongly excite interneurons and identified PV^+ cells as a major subtype of interneurons targeted by the SuM.[5,9] The restricted expression of SuM fibers in the CA1 SR/SLM border (Figures 1C-1E), compared to the more diffusive SuM fibers across all layers in CA3,[5] raises an interesting question of whether the functional connectivity between SuM and CA1 differs from its connection with CA3. We noted that the dendrites of CA1 PV^+ cells do extend to the SR/SLM, raising the possibility of potential physical contacts between SuM fibers and PV^+ dendrites (e.g., Figure 5C). To address the functional connectivity, we generated PV-td mice by crossing a PV-IRES-Cre line with an Ai9 tdTomato reporter line, as described previously (Figures 5A-5C).[5,45] An AAV-Syn-ChR2-EYFP was bilaterally injected into the SuM in PV-td mice, and we performed whole-cell recordings 3–5 weeks after viral injection (Figures 5B-5E). Surprisingly, unlike CA2 or CA3,[5,9] light pulses produced no detectable excitatory synaptic responses in all CA1 PV^+ cells tested (0%, 0/10 cells) (Figures 5E, 5I, and 5J).

Next, we asked whether SuM inputs innervate SOM^+ cells, another major subtype of CA1 interneurons. We used a similar approach to identify SOM^+ cells by crossing a SOM-IRES-Cre line with an Ai9 tdTomato reporter line (Figures 5A, 5B, and 5F-5H). We found that none of the CA1 SOM^+ cells received the excitatory synaptic responses from the SuM (0%, 0/9 cells, Figures 5H and 5I). This result was somewhat expected, as very few SuM fibers are present in the stratum oriens (SO), where most dendrites of SOM^+ cells are located. Taking these results together, we conclude that the SuM completely avoids two major subtypes of CA1 interneurons, PV^+ and SOM^+ cells.

In summary, the connectivity probabilities between the SuM and different CA1 interneuron subtypes vary substantially (Figure 5I). The connectivity probabilities between the SuM and SR/SLM interneurons in general and between the SuM and VIP^+ cells were very high, followed by $NDNF^+$ cells, whereas PV^+ and SOM^+ cells did not receive the monosynaptic excitation from the SuM (Figure 5I). In addition, optogenetic stimulation of SuM terminals

evoked APs in most SR/SLM interneurons and VIP$^+$ cells but failed to evoke APs in NDNF$^+$, PV$^+$, or SOM$^+$ cells (Figure 5J).

Most nonresponsive cells are presumably NDNF$^+$ cells

We noted that approximately 22.2% of CA1 SR/SLM interneurons (10/45 cells) during "random" patch-clamp recording did not show any detectable light-evoked excitatory responses (nonresponsive cells) (Figure 2L). Given that NDNF$^+$ cells have relatively lower connectivity probability and none of them fire spikes in response to SuM stimulation (Figures 3H and 3I), we asked whether most nonresponsive cells were indeed NDNF$^+$ cells. To test this possibility, we analyzed and compared basic electrical properties of three groups: responsive, nonresponsive, and NDNF$^+$ (Figure S3). We found that the parameters of passive and active membrane properties of nonresponsive cells were largely comparable to those of NDNF$^+$ cells but significantly differed from responsive cells (Figure S3). For example, responsive cells had significantly more depolarized resting membrane potentials than nonresponsive or NDNF cells (responsive, −50.6 ± 1.0 mV, n = 35 cells; nonresponsive, −60.8 ± 2.9 mV, n = 9 cells; NDNF$^+$, −62.4 ± 1.1 mV, n = 20 cells; $p = 4.64 \times 10^{-8}$, one-way ANOVA). In addition, the parameters of AP wave-forms, including AP amplitude, rise time, half-width, and decay time, in nonresponsive cells were comparable to those of NDNF$^+$ cells, but were substantially different from those of responsive cells (Figure S3). For example, responsive cells had a significantly shorter AP half-width than nonresponsive or NDNF cells (responsive, 0.419 ± 0.025 ms, n = 35 cells; nonresponsive, 0.673 ± 0.081 ms, n = 9 cells; NDNF$^+$, 0.701 ± 0.022 ms, n = 20 cells; $p = 6 \times 10^{-9}$, one-way ANOVA). Overall, the electrical properties of nonresponsive cells closely match those of NDNF$^+$ cells but significantly differ from those of responsive cells. Although not conclusive, these results indicate that the nonresponsive cells likely comprise a relatively homogeneous group of interneurons, presumably corresponding to a subset of NDNF$^+$ cells (neurogliaform cells).

The SuM provides no direct excitation but provides feedforward inhibition to suppress CA1 PNs

Finally, we asked: does the SuM make monosynaptic connections with CA1 PNs? What is the impact of SuM activation on CA1 PNs? To address these questions, we bilaterally injected AAV-Syn-ChR2-EYFP into the SuM and performed whole-cell recording in CA1 PNs (Figures 6A-6C). Voltage-clamp recording showed that light pulses produced no excitatory synaptic responses in any of the CA1 PNs tested (0%, 0/20 cells) while holding the membrane potential at −70 mV (near reversal potential of inhibition), indicating the complete absence of direct monosynaptic excitation between the SuM and the CA1 PNs (Figures 6D and 6J). Interestingly, light pulses consistently produced an outward current (IPSC) in CA1 PNs when the membrane was held at −50 mV (10.8 ± 2.9 pA, n = 10 cells) (Figure 6D). Similarly, in current clamp, we found very little change in membrane potential when light pulses were delivered at the resting potential (Figures 6E and 6F). Remarkably, when a small constant positive current was injected to depolarize the membrane potential to near −50 mV, light stimulation produced a small, but consistent, membrane hyperpolarization (−1.72 ± 0.43 mV, n = 13 cells, Figures 6E and 6F). Overall, in all CA1 PNs tested, we detected no light-evoked excitatory synaptic connections (0%, 0/20 cells, Figure 6J). In sharp contrast, the light-evoked inhibitory events (IPSCs or inhibitory

postsynaptic potentials, IPSPs) were detected in an overwhelming majority of CA1 PNs tested (95%, 19/20 cells, Figure 6J). Moreover, the onset of the inhibitory events in CA1 PNs was substantially longer than the onset of EPSCs in CA1 interneurons (Figure 6G, IN-excitation, 1.13 ± 0.07 ms, $n = 35$ cells; PN-inhibition, 6.00 ± 0.38 ms, $n = 14$ cells; $p = 3.2 \times 10^{-23}$, unpaired t test). In addition, light-evoked IPSCs were completely abolished by bath application of DNQX/APV (Figures 6H and 6I, DNQX/APV = 3.93 ± 1.61% of baseline, $n = 5$ cells/3 mice; $p = 0.00183$, paired t test). These results suggest that the light-evoked inhibition in CA1 PNs is mediated by disynaptic feedforward driven by spikes of SR/SLM interneurons.

Next, we directly assessed the impact of the SuM-driven feedforward inhibition on CA1 PN excitability. A 10 Hz light stimulation protocol led to minimal changes in membrane potential at resting potential in CA1 PNs but a significantly hyperpolarized membrane potential when the membrane potential was depolarized to near −50 mV (Figures 6K and 6L). Finally, we used a protocol of injecting a 2 s constant current to elicit APs in CA1 PNs, paired with or without 10 Hz light stimulation (Figures 6M and 6N). We found that 10 Hz light stimulation significantly reduced the number of spikes compared with no light stimulation (Figures 6M and 6N, no light, 12.54 ± 0.46 spikes; light, 8.74 ± 0.77 spikes; $n = 9$ cells; $p = 0.0022$, paired t test). From these results taken together, we conclude that SuM activation was able to suppress CA1 PN excitability by exciting CA1 SR/SLM interneurons.

DISCUSSION

In this study, we provide several conceptual advances in our understanding of the subcortical-hippocampal interactions and SuM-CA1 interneuron circuit. First, the present study provides compelling anatomic and functional evidence that the SuM can directly regulate the activity of CA1, the main output region of the hippocampus, bypassing CA2, CA3, and the DG. Our findings complement the previous work on the SuM-hippocampus circuit, which has thus far almost exclusively focused on the projections from the SuM to CA2 or the DG.[1,6-14,16,21] Second, our data reveal a circuit mechanism by which the SuM regulates CA1 via its selective projection to CA1 SR/SLM interneurons. This is distinct from its actions in CA2 and the DG.[9,13] In CA1, the SuM fibers project to and excite a selective group of interneurons located in the SR/SLM border but completely avoid CA1 PNs, PV^+ cells, and SOM^+ cells. By contrast, in CA2 and the DG, the SuM fibers project heavily to the pyramidal cell layer or GCL and target both excitatory and inhibitory neurons.[9,13] Third, we demonstrated that one function of this pathway is for the SuM to suppress CA1 PN activity via feedforward inhibition. In addition, given that both CA1 interneurons and the SuM are involved in generating hippocampal rhythmic activity, such as theta oscillations,[2,15,46,47] our results raise an interesting possibility that this SuM-CA1 interneuron pathway may play an important role in coordinating rhythmic activity between the hippocampus and the SuM in behaving animals. Finally, it has been well established that entorhinal cortex layer III and the thalamic nucleus reuniens are the two major excitatory sources projecting to the CA1 SLM and make synaptic contacts with both CA1 PNs and interneurons.[48,49] The SuM-CA1 pathway identified here represents another glutamatergic pathway that selectively targets the CA1 SR/SLM, but has distinct postsynaptic targets, compared to other pathways. The preferential innervation of the SuM onto a selective group

of SR/SLM interneurons provides an opportunity to explore the function of this class of less-studied interneurons.[31,34]

Sparse innervation can have significant functional relevance

Over the past decade, the SuM-hippocampus projections have gained significant attention,[1] with intense interest in its projections to the DG and CA2, presumably because of the apparent dense SuM innervation onto both regions. Interestingly, our survey of the published studies using conventional tracing or modern viral tracing consistently reveals the presence of SuM fibers in the CA1 SR/SLM border.[9,12,22,27] Yet, surprisingly, this pathway has received no mention in any prior literature. Our current study, together with our previous work on the SuM-CA3 pathway,[5] raises an important question for the field of anatomic and functional neural circuit mapping: seemingly sparse innervation in downstream targets should not be neglected. The level of fiber density, which is often used as a proxy for connectivity strength, may not necessarily correlate with the functional significance under certain conditions. The present study represents a striking example highlighting the importance of identifying the target cell types and evaluating connectivity at the functional level. Notably, in both SuM-CA1 and SuM-CA3 pathways, the SuM selectively targets interneurons.[5] As the number of interneurons is small, sparse afferents would be sufficient to cause a great number of interneurons to fire APs. Because each interneuron can make thousands of synaptic contacts with a large number of downstream principal neurons and other interneurons,[29,30] the disynaptic inhibitory signal can be broadcasted and amplified to a larger area. This view is supported by our observation here as well as our previous report on the SuM-CA3 pathway.[5] Nearly all CA1 and CA3 PNs are regulated by the SuM-driven disynaptic inhibition. Thus, under certain conditions the sparse innervation can potentially have a significant impact on the downstream region.

Selective targeting of CA1 SR/SLM interneurons by the SuM

Our results demonstrated that an extrahippocampal glutamatergic pathway selectively targets a group of interneurons in the CA1 SR/SLM border and completely avoids making monosynaptic connections with CA1 PNs. The SuM fiber trajectory within a narrow band in the CA1 SR/SLM border is striking, if not unique. Its geometric location indicates that SuM fibers are strategically positioned to target SR/SLM interneurons, whose cell bodies and dendrites are concentrated in the SR/SLM border. Of note, CA1 SR/SLM interneurons are highly diverse but remain relatively underexplored, compared to interneurons in other layers, such as PV^+ and SOM^+ cells in the SO and SP.[29-31]

Our data show that the SuM is highly selective in targeting specific cell types in CA1, which is markedly distinct from its projection to CA2, CA3, and the DG. First, unlike its dense projection to CA2 and the DG, where nearly all principal neurons receive monosynaptic inputs,[5,9,13] SuM inputs completely avoid CA1 PNs but selectively target CA1 interneurons. Second, in sharp contrast with its preferential innervation onto PV^+ cells in CA2 and CA3,[5,9] the SuM completely avoids making monosynaptic connections with PV^+ cells in CA1. Third, even within the CA1 SR/SLM interneurons, the SuM projection does not appear to randomly target SR/SLM interneurons. Based on their electrophysiological properties, the cells that do not receive SuM inputs can be classified into a relatively homogeneous

group of interneurons. Our analysis indicates that the electrical properties of nonresponsive cells match those of neurogliaform cells, whereas the connectivity probability of other SR/SLM interneuron subtypes is considerably high. Moreover, our data indicate that VIP^+ cells in SR/SLM received a weaker excitatory input, compared to VIP^- cells. However, the impact of SuM activation on VIP^+ cells, measured by the high probability of firing in response to repetitive SuM stimulation, is still significant. This is likely, in part, due to the high input resistance in VIP^+ cells. The genetic identity of VIP^- or $NDNF^-$ cells that were strongly excited by the SuM is unknown. Based on the previous studies on CA1 SR/SLM interneurons,[31,32,34] they likely comprise a diverse group of interneurons that express cholecystokinin (CCK) and/or other interneuron markers and preferentially target different dendritic compartments in CA1 PNs (see below).

Functional implications of the SuM-CA1 interneuron pathway

We show that SuM activation powerfully excites CA1 SR/SLM interneurons to fire APs, which is sufficient to suppress CA1 PN excitability. Notably, CA1 SR/SLM interneurons are highly heterogeneous, and unlike perisomatic inhibition mediated by basket cells, different subtypes of SR/SLM interneurons preferentially target different dendritic compartments in CA1 PNs, including apical dendrites in both SR and SLM and basal dendrites in SO.[31,32,38,39] Given that SuM activation can cause most SR/SLM interneurons to fire APs, the level of somatic suppression in CA1 PNs induced by SuM activation was surprisingly moderate. This moderate somatic inhibition can be explained by the preferred dendritic targeting of SR/SLM interneurons,[31,32] as dendritic inhibition cannot be accurately measured at the soma. Thus, we propose that the SuM-CA1 pathway is well positioned to regulate CA1 dendritic excitability and powerfully gate two primary excitatory drives from CA2/CA3 (Schaffer collateral) and the entorhinal cortex (perforant path). Future studies using dendritic patch-clamp recording will be valuable to further explore whether SuM inputs can regulate dendritic excitability and integration in CA1 PNs.

The SuM is involved in multiple hippocampal-dependent behaviors, including spatial learning and social behavior, with each of these functions being assigned to its respective projections to either the DG or CA2.[1] Our findings indicate that the current view of the functions of the SuM-DG versus the SuM-CA2 pathway is likely overly simplistic, given that CA1 and CA3 are also involved in spatial memory and social behavior.[28,50-53] We argue that a holistic view including SuM-CA1 and SuM-CA3 projections is required to interpret functions of the SuM-hippocampus circuit.

Limitations of the study

One technical limitation using AAVretro-Cre (Figures 1F-1I) is the potential leakage of the virus to the neighboring CA2/3 or DG. The leakage could explain the presence of $ChR2\text{-}EYFP^+$ fibers in CA2 and DG in Figures 1H and 1I. Additional work is required to examine whether the SuM neurons that project to CA1 represent a subtype distinct from those projecting to other hippocampal regions.

Although we have identified VIP^+ and $NDNF^+$ cells as two sub-types of interneurons targeted by the SuM, the excitatory synaptic responses in these two cell types were relatively

weak. The genetic identity of the strong responsive interneurons is unknown. Additional work using other interneuron-specific mouse lines is needed to identify the large responsive cell types. In addition, although our study provides important insights into an SuM-CA1 circuit at the anatomic and functional levels, the *in vivo* behavioral relevance of this circuit is unknown. The SuM is thought to act as an important theta oscillator.[1,2,14,15,19,46,54,55] Different subtypes of hippocampal interneurons are also involved in generating rhythmic activity, including theta and gamma oscillations.[46,47,56] This raises an interesting possibility that the SuM-CA1 interneuron pathway may play a role in coordinating activity between the SuM and the hippocampus during rhythmic activity in behaving animals. This idea remains to be tested in the future.

STARMETHODS

EXPERIMENTAL MODEL AND STUDY PARTICIPANT DETAILS

Animals—All mouse lines, including PV-IRES-Cre (stock number: 017320), SOM-IRES-Cre (stock number: 028864), VIP-IRES-Cre (stock number: 031628), NDNF-IRES-Cre (stock number: 030757), and Ai9 tdTomato reporter (stock number: 007909), were purchased from the Jackson Laboratory (JAX). Mice were housed and bred in the Animal Resource Center of Case Western Reserve University School of Medicine on a 12h/12h, light/dark cycle with *ad libitum* access to food and water. Both male and female mice of 2–5-month-old with C57BL6 background were used in the experiments. The procedures described were conducted in accordance with National Institutes of Health regulations and approved by the Institutional Animal Care and Use Committees of Case Western Reserve University.

Hippocampal slice preparation—Transverse hippocampal slices were prepared from 2–5-month-old mice.[5,45] Animals were anesthetized with isoflurane and sacrificed by decapitation in accordance with institutional regulations. Both left and right hippocampi were immediately dissected out from the mouse brain on ice and the entire hippocampus were embedded in a block of premade agar (3-4%). The transverse hippocampal slices (400 μm thick) were then cut from dorsal to ventral on Leica VT1000s or VT1200s vibratomes (Leica Biosystems, Germany) in ice-cold dissection solution containing (in mM): 10 NaCl, 195 sucrose, 2.5 KCl, 10 glucose, 25 $NaHCO_3$, 1.25 NaH_2PO_4, 2 Na-Pyruvate, 0.5 $CaCl_2$ and 7 $MgCl_2$. Only dorsal slices (dorsal 20-50%) were used in this study. Slices were then incubated at 32°C in regular artificial cerebrospinal fluid (ACSF in mM: 125 NaCl, 2.5 KCl, 20 glucose, 25 $NaHCO_3$, 1.25 NaH_2PO_4, 2 Na-Pyruvate, 2 $CaCl_2$ and 1 $MgCl_2$) for 20-30 min and then kept at room temperature for at least 1.5 hours before transfer to the recording chamber for patch-clamp recording. Dissection solution and recording ACSF were both saturated with 95% O_2 and 5% CO_2 (pH 7.4). All electrophysiological recordings were performed at 31-32°C.

METHOD DETAILS

Whole-cell patch-clamp recording—Whole-cell recordings were obtained from CA1 PNs using the “blind” patch clamp technique under a 4x objective[5,58,59]. Recordings from interneurons or tdTomato$^+$ cells were obtained using conventional visualized patch clamp

technique under a 40x water-immersion objective. The patch pipettes were pulled from borosilicate capillary glass using a P-1000 Micropipette Puller (Sutter Instruments, Novato, CA, USA) and had resistances ranging from 4 to 6 MU. The pipettes were filled with an intracellular solution of the following chemicals (in mM): 135 K-Gluconate, 5 KCl, 0.1 EGTA-Na, 10 HEPES, 2 NaCl, 5 ATP-Mg, 0.4 GTP-Na2, 10 phosphocreatine-Na2 (pH 7.3-7.4; 280 – 290 mOsm). Biocytin (0.2%) was included in the intracellular solution. Liquid junction potential was not corrected. Series resistance was monitored throughout each experiment. Neurons with a series resistance >30 MΩ were excluded from analysis. Resting membrane potential was measured immediately upon break-in. CA1 PNs with resting potentials more depolarized than −60 mV upon break-in were excluded from analysis. Interneurons with resting potentials more depolarized than −36 mV upon break-in were also excluded from analysis. During voltage-clamp recording, neurons were held at −70 mV or −50 mV for EPSC or IPSC measurements, respectively, whereas PSP and action potentials were measured at resting potential in current-clamp mode. For IPSC measurements in some voltage-clamp experiments (Figures 2H, 2I, 6H, and 6I), Cs+ based intracellular solution was used: 135 Cs Methanesulfonate, 5 KCl, 0.1 EGTA-Na, 10 HEPES, 2 NaCl, 5 ATP-Mg, 0.4 GTP-Na2, 10 phosphocreatine-Na2 (pH 7.3-7.4; 280 – 290 mOsm). In some current-clamp recording experiments, a constant positive current was injected into the soma to depolarize membrane potential to approximately −50 mV in order to reveal hyperpolarizing responses mediated by inhibition.

Optogenetics—The 470-nm blue light pulses were delivered via a 40x water immersion objective placed above the slices through a 4-color LED light source (LED4D294, Thorlabs) driven by pClamp11 software. Photostimuli consisting of 2-ms blue light pulses of maximum light intensity were delivered to evoke light response. A single light pulse or a 10-pulse train of 10-20 Hz light stimulation protocol was applied.

Stereotaxic viral injection—Mice were anesthetized with isoflurane (1-3%) and placed in a digital stereotaxic apparatus (RWD Life Science, Cat. No: 68045). The glass micropipettes pulled from a P-1000 puller (Sutter Instrument) were used for viral injection using a nanoinjector system (Nanoject III, Drummond Scientific)[5,45].

For SuM anterograde tracing, 100 nl AAV8-hSyn-ChR2-EYFP (Salk Viral Vector Core) was injected into the SuM of the WT mice bilaterally using the coordinates (AP: −2.70 mm; ML: ±0.50 mm; DV: −4.80/−5.00 mm). Two weeks later, mice were sacrificed for histology.

To target ChR2-EYFP into SuM neurons that project to CA1, an AAVretro carrying Cre recombinase (AAVretro-EF1α-mCherry-IRES-Cre, 100 nl, Addgene) was unilaterally injected into dorsal CA1 of the WT mice first, using the coordinates (AP: −1.90 mm; ML: +1.50 mm; DV: −1.50 mm). Cre retrogradely spreads to presynaptic SuM neurons that project to CA1. After two weeks, a second Cre-dependent AAV (AAVdj-EF1a-DIO-hChR2-EYFP-WPRE-pA, 100 nl, Salk Viral Vector Core) was injected into SuM bilaterally using the coordinates (AP: −2.80 mm; ML: ±0.40 mm; DV: −4.80 mm) to target CA1-projecting SuM neurons. Mice were sacrificed for histology after two weeks.

For optogenetic stimulation of SuM terminals, rAAV2-hsyn-hChR2(H134R)-EYFP-WPRE-PA (400 nl per site, UNC Viral Core) was injected bilaterally into the SuM of the WT, PV-tdTomato, SOM-tdTomato, VIP-tdTomato, or NDNF-tdTomato mice (AP: −2.80 mm; ML: ±0.40 mm; DV: −4.80 mm). Mice were sacrificed 3-5 weeks after viral injection for electrophysiological recording.

Biocytin staining—Slices that underwent whole-cell recordings were fixed at 4°C for 24–48 hours in 4% PFA in PBS, pH 7.3. The fixed slices were subsequently treated with PBS containing normal goat serum (5%) and 0.5% Triton for 2 hours at room temperature. Slices were then incubated in PBS containing Streptavidin, Alexa Fluor 594 or 647 conjugate (1:500) and 0.1% Triton for 2 days at 4°C. Subsequently, slices were rinsed in PBS several times and embedded in VECTASHIELD Antifade Mounting Medium (Vector Laboratories), followed by fluorescent imaging using a confocal microscope (LSM 800; Zeiss).[5,58]

Immunohistochemistry and confocal microscopy—Mice were deeply anesthetized, perfused with pre-cooling phosphate buffered saline (PBS), followed by 4% paraformaldehyde (PFA) in PBS. Brains were dissected out and post-fixed with 4% PFA overnight at 4°C. Coronal sections (45-μm thick) were cut using Leica 1000-S vibratome. Floating sections were first rinsed three times in 1x PBS and then blocked in 1x PBS with 0.3% Triton X-100 and 5% normal goat serum for 1 hr at room temperature (RT). Incubation with primary antibodies was performed at 4°C overnight in 1 x PBS with 0.3% Triton X-100. The following primary antibodies were used: chicken anti-GFP (1:500, Aves lab, Cat #: GFP-1020). Sections were then washed three times in PBS and incubated with secondary antibodies (goat anti-chicken 488, 1:1000, Invitrogen, Cat #: A11039) for 1-2 hr at room temperature. Sections were then washed three times in PBS and incubated with DAPI for 10-20 min at room temperature. Sections were washed three times in PBS, mounted and embedded in VECTASHIELD Antifade Mounting Medium (Vector Laboratories). The fluorescence images were obtained using a laser scanning confocal microscope (LSM 800; Zeiss) and analyzed in ImageJ Fiji.

QUANTIFICATION AND STATISTICAL ANALYSIS

Student’s t test, one-way ANOVA, or two-way ANOVA test followed by a Tukey test for multiple comparisons were used for statistical analysis. Statistics were analyzed using Excel with Microsoft 365 (Microsoft Corporation, Redmond, WA, USA), Igor Pro 8 software (WaveMetrics, Lake Oswego, OR, USA), or OriginPro 2022b (OriginLab, Northampton, MA, USA). The statistical details of experiments, including the statistical tests used and the values of n, can be found in the figure legends or results. The line profile of fluorescence intensity in Figure 1D was analyzed using “Plot Profile” function in ImageJ Fiji. The values were obtained by drawing a straight line along the CA1 radial axis and the fluorescence intensity was normalized to the peak value for each line. The electrophysiological data were analyzed using in-house functions in AxoGraph X or pClamp 11. All data are expressed as mean ± SEM. $P < 0.05$ is considered statistically significant.

Supplementary Material

Refer to Web version on PubMed Central for supplementary material.

ACKNOWLEDGMENTS

This work was supported by R01MH129294 and R01MH130367 from the NIH (Q.S.) and institutional support from Case Western Reserve University (Q.S.).

REFERENCES

1. Kesner AJ, Mozaffarilegha M, Thirtamara Rajamani K, Arima Y, Harony-Nicolas H, Hashimotodani Y, Ito HT, Song J, and Ikemoto S (2023). Hypothalamic Supramammillary Control of Cognition and Motivation. J. Neurosci 43, 7538–7546. 10.1523/JNEUROSCI.1320-23.2023. [PubMed: 37940587]
2. Pan WX, and McNaughton N (2004). The supramammillary area: its organization, functions and relationship to the hippocampus. Prog. Neurobiol 74, 127–166. 10.1016/j.pneurobio.2004.09.003. [PubMed: 15556285]
3. Pedersen NP, Ferrari L, Venner A, Wang JL, Abbott SBG, Vujovic N, Arrigoni E, Saper CB, and Fuller PM (2017). Supramammillary glutamate neurons are a key node of the arousal system. Nat. Commun 8, 1405. 10.1038/s41467-017-01004-6. [PubMed: 29123082]
4. Renouard L, Billwiller F, Ogawa K, Clément O, Camargo N, Abdelkarim M, Gay N, Scoté-Blachon C, Touré R, Libourel PA, et al. (2015). The supramammillary nucleus and the claustrum activate the cortex during REM sleep. Sci. Adv 1, e1400177. 10.1126/sciadv.1400177. [PubMed: 26601158]
5. Li M, Kinney JL, Jiang YQ, Lee DK, Wu Q, Lee D, Xiong WC, and Sun Q (2023). Hypothalamic Supramammillary Nucleus Selectively Excites Hippocampal CA3 Interneurons to Suppress CA3 Pyramidal Neuron Activity. J. Neurosci 43, 4612–4624. 10.1523/JNEUROSCI.1910-22.2023. [PubMed: 37117012]
6. Li YD, Luo YJ, Xie L, Tart DS, Sheehy RN, Zhang L, Coleman LG Jr., Chen X, and Song J (2023). Activation of hypothalamic-enhanced adult-born neurons restores cognitive and affective function in Alzheimer's disease. Cell Stem Cell 30, 415–432.e6. 10.1016/j.stem.2023.02.006. [PubMed: 37028406]
7. Li YD, Luo YJ, Chen ZK, Quintanilla L, Cherasse Y, Zhang L, Lazarus M, Huang ZL, and Song J (2022). Hypothalamic modulation of adult hippocampal neurogenesis in mice confers activity-dependent regulation of memory and anxiety-like behavior. Nat. Neurosci 25, 630–645. 10.1038/s41593-022-01065-x. [PubMed: 35524139]
8. Qin H, Fu L, Jian T, Jin W, Liang M, Li J, Chen Q, Yang X, Du H, Liao X, et al. (2022). REM sleep-active hypothalamic neurons may contribute to hippocampal social-memory consolidation. Neuron 110, 4000–4014.e6. 10.1016/j.neuron.2022.09.004. [PubMed: 36272414]
9. Robert V, Therreau L, Chevaleyre V, Lepicard E, Viollet C, Cognet J, Huang AJ, Boehringer R, Polygalov D, McHugh TJ, and Piskorowski RA (2021). Local circuit allowing hypothalamic control of hippocampal area CA2 activity and consequences for CA1. Elife 10, e63352. 10.7554/eLife.63352. [PubMed: 34003113]
10. Farrell JS, Lovett-Barron M, Klein PM, Sparks FT, Gschwind T, Ortiz AL, Ahanonu B, Bradbury S, Terada S, Oijala M, et al. (2021). Supramammillary regulation of locomotion and hippocampal activity. Science 374, 1492–1496. 10.1126/science.abh4272. [PubMed: 34914519]
11. Li Y, Bao H, Luo Y, Yoan C, Sullivan HA, Quintanilla L, Wickersham I, Lazarus M, Shih YI, and Song J (2020). Supramammillary nucleus synchronizes with dentate gyrus to regulate spatial memory retrieval through glutamate release. Elife 9, e53129. 10.7554/eLife.53129. [PubMed: 32167473]
12. Chen S, He L, Huang AJY, Boehringer R, Robert V, Wintzer ME, Polygalov D, Weitemier AZ, Tao Y, Gu M, et al. (2020). A hypothalamic novelty signal modulates hippocampal memory. Nature 586, 270–274. 10.1038/s41586-020-2771-1. [PubMed: 32999460]

13. Hashimotodani Y, Karube F, Yanagawa Y, Fujiyama F, and Kano M (2018). Supramammillary Nucleus Afferents to the Dentate Gyrus Corelease Glutamate and GABA and Potentiate Granule Cell Output. Cell Rep. 25, 2704–2715.e4. 10.1016/j.celrep.2018.11.016. [PubMed: 30517859]

14. Ito HT, Moser EI, and Moser MB (2018). Supramammillary Nucleus Modulates Spike-Time Coordination in the Prefrontal-Thalamo-Hippocampal Circuit during Navigation. Neuron 99, 576–587.e5. 10.1016/j.neuron.2018.07.021. [PubMed: 30092214]

15. Pan WX, and McNaughton N (2002). The role of the medial supramammillary nucleus in the control of hippocampal theta activity and behaviour in rats. Eur. J. Neurosci 16, 1797–1809. 10.1046/j.1460-9568.2002.02267.x. [PubMed: 12431233]

16. Ajibola MI, Wu JW, Abdulmajeed WI, and Lien CC (2021). Hypothalamic Glutamate/GABA Cotransmission Modulates Hippocampal Circuits and Supports Long-Term Potentiation. J. Neurosci 41, 8181–8196. 10.1523/JNEUROSCI.0410-21.2021. [PubMed: 34380766]

17. Aranda L, Begega A, Sánchez-López J, Aguirre JA, Arias JL, and Santín LJ (2008). Temporary inactivation of the supramammillary area impairs spatial working memory and spatial reference memory retrieval. Physiol. Behav 94, 322–330. 10.1016/j.physbeh.2008.01.024. [PubMed: 18346765]

18. Shahidi S, Motamedi F, and Naghdi N (2004). Effect of reversible inactivation of the supramammillary nucleus on spatial learning and memory in rats. Brain Res. 1026, 267–274. 10.1016/j.brainres.2004.08.030. [PubMed: 15488489]

19. Pan WX, and McNaughton N (1997). The medial supramammillary nucleus, spatial learning and the frequency of hippocampal theta activity. Brain Res. 764, 101–108. 10.1016/s0006-8993(97)00431-9. [PubMed: 9295198]

20. Thirtamara Rajamani K, Barbier M, Lefevre A, Niblo K, Cordero N, Netser S, Grinevich V, Wagner S, and Harony-Nicolas H (2024). Oxytocin activity in the paraventricular and supramammillary nuclei of the hypothalamus is essential for social recognition memory in rats. Mol. Psychiatry 29, 412–424. 10.1038/s41380-023-02336-0. [PubMed: 38052983]

21. Tabuchi E, Sakaba T, and Hashimotodani Y (2022). Excitatory selective LTP of supramammillary glutamatergic/GABAergic cotransmission potentiates dentate granule cell firing. Proc. Natl. Acad. Sci. USA 119, e2119636119. 10.1073/pnas.2119636119. [PubMed: 35333647]

22. Haglund L, Swanson LW, and Köhler C (1984). The projection of the supramammillary nucleus to the hippocampal formation: an immunohisto-chemical and anterograde transport study with the lectin PHA-L in the rat. J. Comp. Neurol 229, 171–185. 10.1002/cne.902290204. [PubMed: 6501599]

23. Soussi R, Zhang N, Tahtakran S, Houser CR, and Esclapez M (2010). Heterogeneity of the supramammillary-hippocampal pathways: evidence for a unique GABAergic neurotransmitter phenotype and regional differences. Eur. J. Neurosci 32, 771–785. 10.1111/j.1460-9568.2010.07329.x. [PubMed: 20722723]

24. Vertes RP (2015). Major diencephalic inputs to the hippocampus: supramammillary nucleus and nucleus reuniens. Circuitry and function. Prog. Brain Res 219, 121–144. 10.1016/bs.pbr.2015.03.008. [PubMed: 26072237]

25. Nakanishi K, Saito H, and Abe K (2001). The supramammillary nucleus contributes to associative EPSP-spike potentiation in the rat dentate gyrus in vivo. Eur. J. Neurosci 13, 793–800. 10.1046/j.1460-9568.2001.01446.x. [PubMed: 11207814]

26. Carre GP, and Harley CW (1991). Population spike facilitation in the dentate gyrus following glutamate to the lateral supramammillary nucleus. Brain Res. 568, 307–310. 10.1016/0006-8993(91)91415-w. [PubMed: 1687670]

27. Vertes RP (1992). PHA-L analysis of projections from the supramammillary nucleus in the rat. J. Comp. Neurol 326, 595–622. 10.1002/cne.903260408. [PubMed: 1484125]

28. Tsien JZ, Huerta PT, and Tonegawa S (1996). The essential role of hippocampal CA1 NMDA receptor-dependent synaptic plasticity in spatial memory. Cell 87, 1327–1338. 10.1016/s0092-8674(00)81827-9. [PubMed: 8980238]

29. Pelkey KA, Chittajallu R, Craig MT, Tricoire L, Wester JC, and McBain CJ (2017). Hippocampal GABAergic Inhibitory Interneurons. Physiol. Rev 97, 1619–1747. 10.1152/physrev.00007.2017. [PubMed: 28954853]

30. Freund TF, and Buzsáki G (1996). Interneurons of the hippocampus. Hippocampus 6, 347–470. 10.1002/(SICI)1098-1063(1996)6:4<347::AID-HIPO1>3.0.CO;2-I. [PubMed: 8915675]

31. Capogna M (2011). Neurogliaform cells and other interneurons of stratum lacunosum-moleculare gate entorhinal-hippocampal dialogue. J. Physiol 589, 1875–1883. 10.1113/jphysiol.2010.201004. [PubMed: 21135049]

32. Vida I, Halasy K, Szinyei C, Somogyi P, and Buhl EH (1998). Unitary IPSPs evoked by interneurons at the stratum radiatum-stratum lacunosum-moleculare border in the CA1 area of the rat hippocampus in vitro. J. Physiol 506, 755–773. 10.1111/j.1469-7793.1998.755bv.x. [PubMed: 9503336]

33. Harris KD, Hochgerner H, Skene NG, Magno L, Katona L, Bengtsson Gonzales C, Somogyi P, Kessaris N, Linnarsson S, and Hjerling-Leffler J (2018). Classes and continua of hippocampal CA1 inhibitory neurons revealed by single-cell transcriptomics. PLoS Biol. 16, e2006387. 10.1371/journal.pbio.2006387. [PubMed: 29912866]

34. Klausberger T, and Somogyi P (2008). Neuronal diversity and temporal dynamics: the unity of hippocampal circuit operations. Science 321, 53–57. 10.1126/science.1149381. [PubMed: 18599766]

35. Sun Y, Nguyen AQ, Nguyen JP, Le L, Saur D, Choi J, Callaway EM, and Xu X (2014). Cell-type-specific circuit connectivity of hippocampal CA1 revealed through Cre-dependent rabies tracing. Cell Rep. 7, 269–280. 10.1016/j.celrep.2014.02.030. [PubMed: 24656815]

36. Tervo DGR, Hwang BY, Viswanathan S, Gaj T, Lavzin M, Ritola KD, Lindo S, Michael S, Kuleshova E, Ojala D, et al. (2016). A Designer AAV Variant Permits Efficient Retrograde Access to Projection Neurons. Neuron 92, 372–382. 10.1016/j.neuron.2016.09.021. [PubMed: 27720486]

37. Overstreet-Wadiche L, and McBain CJ (2015). Neurogliaform cells in cortical circuits. Nat. Rev. Neurosci 16, 458–468. 10.1038/nrn3969. [PubMed: 26189693]

38. Price CJ, Cauli B, Kovacs ER, Kulik A, Lambolez B, Shigemoto R, and Capogna M (2005). Neurogliaform neurons form a novel inhibitory network in the hippocampal CA1 area. J. Neurosci 25, 6775–6786. 10.1523/JNEUROSCI.1135-05.2005. [PubMed: 16033887]

39. Tricoire L, Pelkey KA, Erkkila BE, Jeffries BW, Yuan X, and McBain CJ (2011). A blueprint for the spatiotemporal origins of mouse hippocampal interneuron diversity. J. Neurosci 31, 10948–10970. 10.1523/JNEUROSCI.0323-11.2011. [PubMed: 21795545]

40. Mercier MS, Magloire V, Cornford JH, and Kullmann DM (2022). Long-term potentiation in neurogliaform interneurons modulates excitation-inhibition balance in the temporoammonic pathway. J. Physiol 600, 4001–4017. 10.1113/JP282753. [PubMed: 35876215]

41. Tricoire L, Pelkey KA, Daw MI, Sousa VH, Miyoshi G, Jeffries B, Cauli B, Fishell G, and McBain CJ (2010). Common origins of hippocampal Ivy and nitric oxide synthase expressing neurogliaform cells. J. Neurosci 30, 2165–2176. 10.1523/JNEUROSCI.5123-09.2010. [PubMed: 20147544]

42. Acsady L, Arabadzisz D, and Freund TF (1996). Correlated morphological and neurochemical features identify different subsets of vasoactive intestinal polypeptide-immunoreactive interneurons in rat hippocampus. Neuroscience 73, 299–315. 10.1016/0306-4522(95)00610-9. [PubMed: 8783251]

43. Guet-McCreight A, Skinner FK, and Topolnik L (2020). Common Principles in Functional Organization of VIP/Calretinin Cell-Driven Disinhibitory Circuits Across Cortical Areas. Front. Neural Circuits 14, 32. 10.3389/fncir.2020.00032. [PubMed: 32581726]

44. Taniguchi H, He M, Wu P, Kim S, Paik R, Sugino K, Kvitsiani D, Fu Y, Lu J, Lin Y, et al. (2011). A resource of Cre driver lines for genetic targeting of GABAergic neurons in cerebral cortex. Neuron 71, 995–1013. 10.1016/j.neuron.2011.07.026. [PubMed: 21943598]

45. Sun Q, Sotayo A, Cazzulino AS, Snyder AM, Denny CA, and Siegelbaum SA (2017). Proximodistal Heterogeneity of Hippocampal CA3 Pyramidal Neuron Intrinsic Properties, Connectivity, and Reactivation during Memory Recall. Neuron 95, 656–672.e3. 10.1016/j.neuron.2017.07.012. [PubMed: 28772124]

46. Buzsaki G (2002). Theta oscillations in the hippocampus. Neuron 33, 325–340. 10.1016/s0896-6273(02)00586-x. [PubMed: 11832222]

47. Bezaire MJ, Raikov I, Burk K, Vyas D, and Soltesz I (2016). Interneuronal mechanisms of hippocampal theta oscillations in a full-scale model of the rodent CA1 circuit. Elife 5, e18566. 10.7554/eLife.18566. [PubMed: 28009257]
48. Goswamee P, Leggett E, and McQuiston AR (2021). Nucleus Reuniens Afferents in Hippocampus Modulate CA1 Network Function via Monosynaptic Excitation and Polysynaptic Inhibition. Front. Cell. Neurosci 15, 660897. 10.3389/fncel.2021.660897. [PubMed: 34712120]
49. Bilash OM, Chavlis S, Johnson CD, Poirazi P, and Basu J (2023). Lateral entorhinal cortex inputs modulate hippocampal dendritic excitability by recruiting a local disinhibitory microcircuit. Cell Rep. 42, 111962. 10.1016/j.celrep.2022.111962. [PubMed: 36640337]
50. Meira T, Leroy F, Buss EW, Oliva A, Park J, and Siegelbaum SA (2018). A hippocampal circuit linking dorsal CA2 to ventral CA1 critical for social memory dynamics. Nat. Commun 9, 4163. 10.1038/s41467-018-06501-w. [PubMed: 30301899]
51. Okuyama T, Kitamura T, Roy DS, Itohara S, and Tonegawa S (2016). Ventral CA1 neurons store social memory. Science 353, 1536–1541. 10.1126/science.aaf7003. [PubMed: 27708103]
52. Chiang MC, Huang AJY, Wintzer ME, Ohshima T, and McHugh TJ (2018). A role for CA3 in social recognition memory. Behav. Brain Res 354, 22–30. 10.1016/j.bbr.2018.01.019. [PubMed: 29355673]
53. Nakashiba T, Young JZ, McHugh TJ, Buhl DL, and Tonegawa S (2008). Transgenic inhibition of synaptic transmission reveals role of CA3 output in hippocampal learning. Science 319, 1260–1264. 10.1126/science.1151120. [PubMed: 18218862]
54. Hernandez-Perez JJ, Gutierrez-Guzman BE, Lopez-Vazquez MA, and Olvera-Cortes ME (2015). Supramammillary serotonin reduction alters place learning and concomitant hippocampal, septal, and supramammillar theta activity in a Morris water maze. Front. Pharmacol 6, 250. 10.3389/fphar.2015.00250. [PubMed: 26578960]
55. McNaughton N, Logan B, Panickar KS, Kirk IJ, Pan WX, Brown NT, and Heenan A (1995). Contribution of synapses in the medial supramammillary nucleus to the frequency of hippocampal theta rhythm in freely moving rats. Hippocampus 5, 534–545. 10.1002/hipo.450050605. [PubMed: 8646280]
56. Colgin LL (2016). Rhythms of the hippocampal network. Nat. Rev. Neurosci 17, 239–249. 10.1038/nrn.2016.21. [PubMed: 26961163]
57. Fenno LE, Mattis J, Ramakrishnan C, Hyun M, Lee SY, He M, Tucciarone J, Selimbeyoglu A, Berndt A, Grosenick L, et al. (2014). Targeting cells with single vectors using multiple-feature Boolean logic. Nat. Methods 11, 763–772. 10.1038/nmeth.2996. [PubMed: 24908100]
58. Sun Q, Jiang YQ, and Lu MC (2020). Topographic heterogeneity of intrinsic excitability in mouse hippocampal CA3 pyramidal neurons. J. Neurophysiol 124, 1270–1284. 10.1152/jn.00147.2020. [PubMed: 32937083]
59. Sun Q, Buss EW, Jiang YQ, Santoro B, Brann DH, Nicholson DA, and Siegelbaum SA (2021). Frequency-dependent synaptic dynamics differentially tune CA1 and CA2 pyramidal neuron responses to cortical input. J. Neurosci 41, 8103–8110. 10.1523/JNEUROSCI.0451-20.2021. [PubMed: 34385360]

Highlights

- The supramammillary nucleus (SuM) projects to the SR/SLM border in hippocampal CA1
- The SuM monosynaptically excites SR/SLM interneurons, including VIP^+ and $NDNF^+$ cells
- The SuM makes no synaptic contacts with CA1 pyramidal neurons (PNs) or PV^+ or SOM^+ cells
- The SuM drives disynaptic feedforward inhibition to suppress CA1 PN excitability

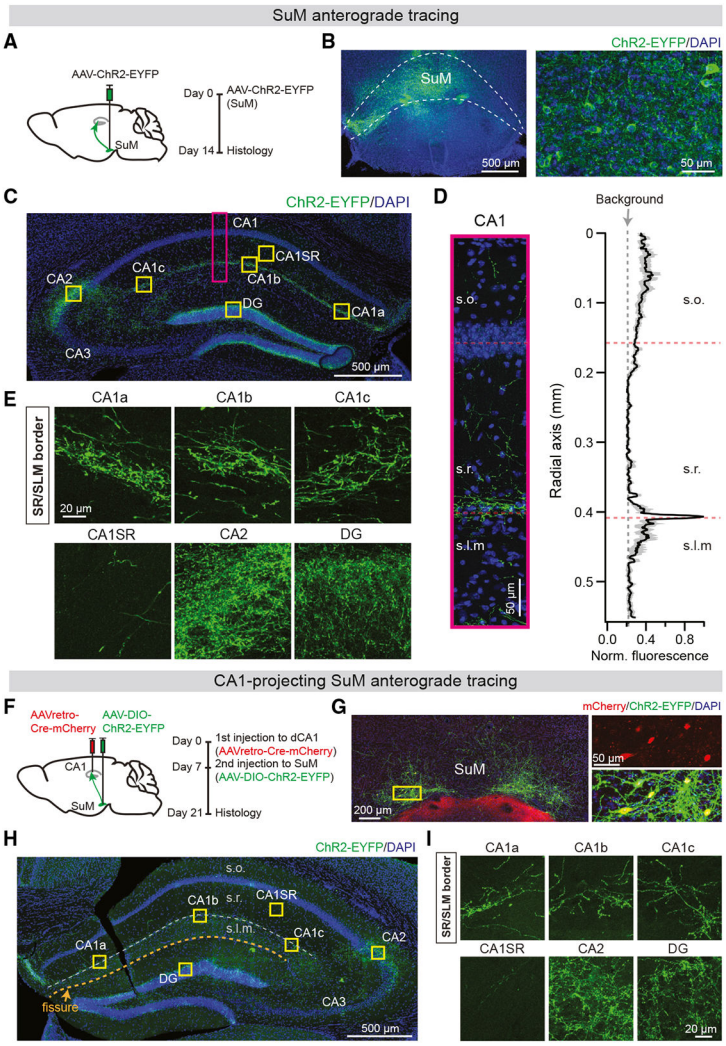

Figure 1. Anatomic evidence of the projection from the SuM to CA1

(A) Experimental procedure and timeline. Schematic of SuM-CA1 projection and injection of AAVSyn-ChR2-EYFP into the SuM.

(B) Sample confocal images show the injection site in the SuM (left) and the expanded view (right).

(C) ChR2-EYFP^{+} fiber distribution in the hippocampus. Note the dense ChR2-EYFP^{+} fibers in the DG and CA2 and in a narrow band between the SR and the SLM in CA1.

(D) Left, expanded view of the rectangle in CA1b shown in (C). Right, quantification of ChR2-EYFP fluorescence intensity along the CA1 radial axis. Note the sharp peak of fluorescence intensity in the SR/SLM border. Gray shading shows the SEM. $n = 6$ slices/4 mice. s.o., stratum oriens; s.r., stratum radiatum; s.l.m., stratum lacunosum-moleculare.

(E) Expanded views of the yellow squares shown in (C). Note the abundant expression of EYFP^{+} fibers in the SR/SLM border along the CA1 transverse axis.

(F) Experimental procedure and timeline show the strategy to target ChR2-EYFP into CA1-projecting SuM neurons.

(G) Left, sample confocal image shows the expression of ChR2-EYFP in the SuM, the injection site of Cre-dependent AAV-DIO-ChR2-EYFP. Right, expanded views show co-labeling of Cre-mCherry and ChR2-EYFP in SuM cells.
(H) The distribution of ChR2-EYFP$^+$ SuMfibers in the hippocampus.
(I) Expanded views of the yellow squares shown in (H). Note the expression of EYFP$^+$ fibers in the SR/SLM border along the CA1 transverse axis. Repeated in four mice.

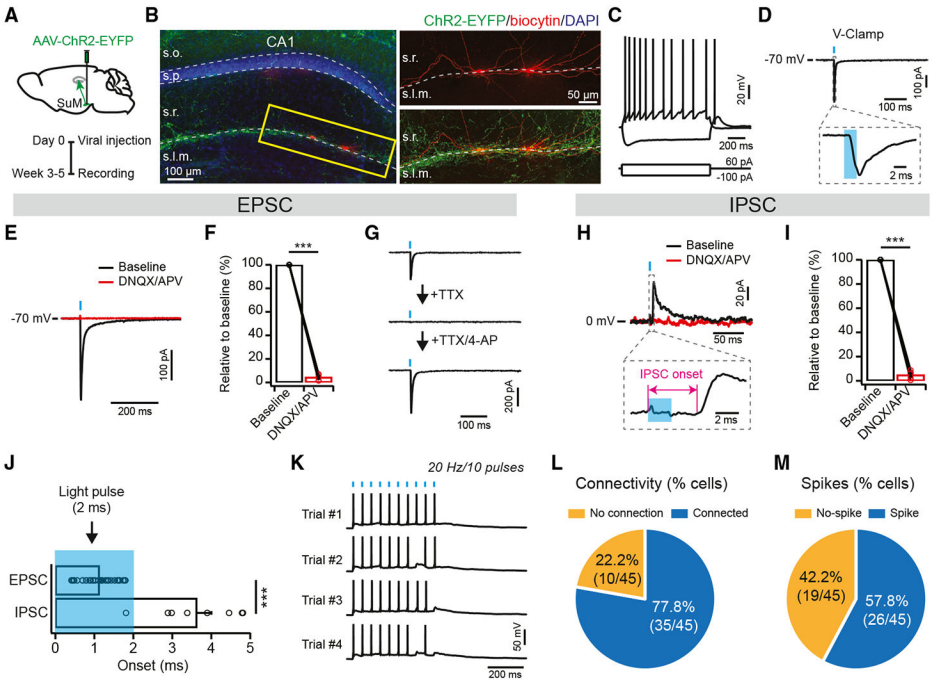

Figure 2. The SuM strongly excites interneurons in the CA1 SR/SLM border

(A) Experimental procedure and timeline.

(B) Representative confocal images showing a hippocampal slice that was injected with AAV-ChR2-EYFP into the SuM and underwent whole-cell recording (left) and expanded views of two biocytin-filled SR/SLM interneurons (right).

(C) Current-clamp recording shows the membrane voltage responses to 1 s somatic injections of the indicated currents from a CA1 SR/SLM interneuron.

(D) Top, voltage-clamp recording shows light-evoked EPSC recorded from a CA1 SR/SLM interneuron (holding potential −70 mV). Bottom, expanded view of the dashed box indicated in the top. Note the very short delay of the onset of EPSC evoked by blue light. Blue bars represent light pulses.

(E and F) Sample traces (E) and group data (F) of light-evoked EPSCs in the absence and presence of DNQX (20 μM) and APV (50 μM). ***$p < 0.001$, paired t test, $n = 5$ cells/3 mice. Error bars show SEM.

(G) Sample voltage-clamp traces show the baseline light-evoked EPSC (top), after bath application of TTX (1 μM) (middle), and followed by bath application of both TTX (1 μM) and 4-AP (1 mM) (bottom). Repeated in three cells.

(H and I) Sample traces (H) and group data (I) of light-evoked IPSCs in the absence and presence of DNQX/APV (holding potential 0 mV). ***$p < 0.001$, paired t test, $n = 6$ cells/3 mice. Error bars show SEM.

(J) Group data of onsets of excitatory synaptic events ($n = 35$ cells/9 mice) versus inhibitory synaptic events in CA1 SR/SLM interneurons ($n = 8$ cells/3 mice). Blue bar depicts the duration of light pulse. ***$p < 0.001$, unpaired t test. Error bars show SEM.

(K) Sample traces of APs evoked by a train of 20 Hz light stimulation in an SR/SLM interneuron.

(L) A pie chart showing the probability of synaptic connections between SuM and CA1 SR/SLM interneurons (n = 45 cells/9 mice).
(M) A pie chart showing the probability of suprathreshold APs evoked by 10–20 Hz light stimulation in CA1 SR/SLM interneurons (n = 45 cells/9 mice).

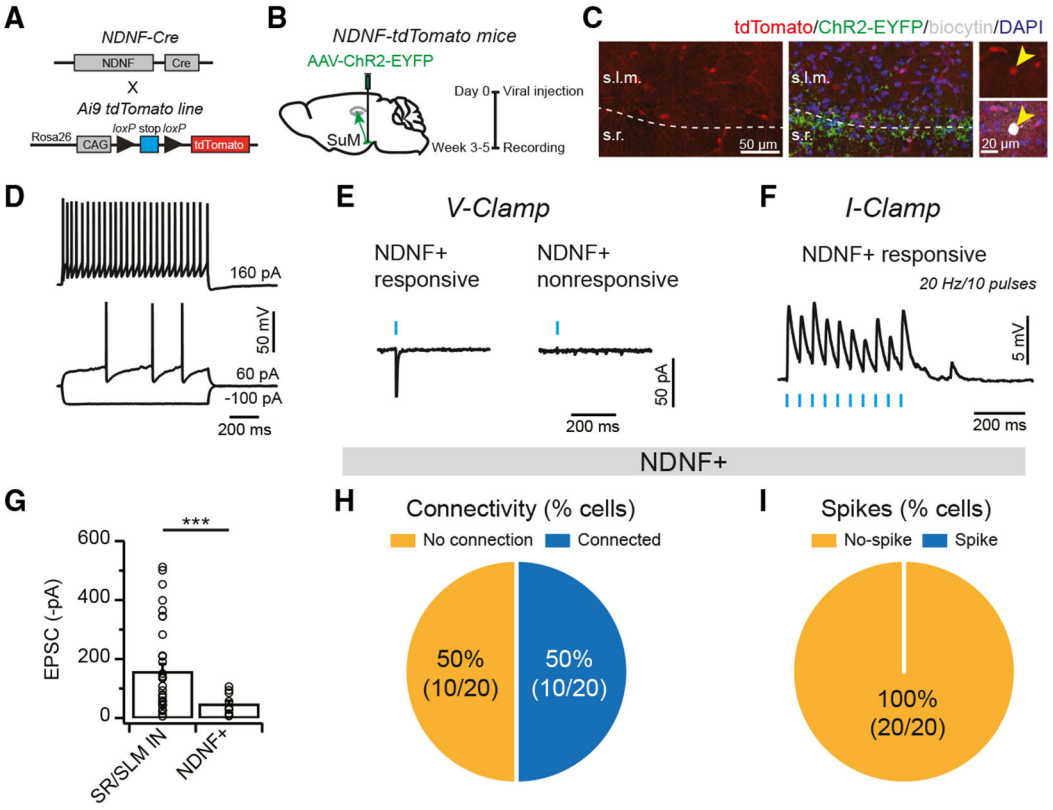

Figure 3. The SuM excites but fails to evoke spikes in NDNF$^+$ cells

(A) Genetic strategy to target tdTomato into NDNF$^+$ cells by crossing an NDNF-IRES-Cre line with a floxed tdTomato reporter line (Ai9).

(B) Experimental procedure and timeline.

(C) Left, the distribution of NDNF$^+$ cells in the CA1 SLM and SR/SLM border. Right, representative confocal images show a biocytin-filled tdTomato$^+$ cell in CA1 from the NDNF-td mouse that underwent whole-cell recording.

(D) Current-clamp recording shows the membrane voltage responses to 1 s somatic injections of the indicated currents from an NDNF$^+$ cell.

(E) Voltage-clamp recording shows sample light-evoked EPSC traces recorded from responsive and nonresponsive NDNF$^+$ cells (holding potential −70 mV).

(F) Sample current-clamp trace of subthreshold postsynaptic potentials (PSPs) evoked by a train of 20 Hz light stimulation from a responsive NDNF$^+$ cell.

(G) Group data of light-evoked EPSCs from CA1 SR/SLM interneurons (n = 35 cells/9 mice) and NDNF$^+$ cells (n = 10 cells/3 mice). ***$p < 0.001$, unpaired t test. Error bars show SEM.

(H) A pie chart shows the probability of connectivity between SuMand NDNF$^+$ cells (n = 20 cells/4 mice).

(I) A pie chart shows that NDNF$^+$ cells (n = 20/20 cells/4 mice) do not fire suprathreshold APs evoked by 10–20 Hz light stimulation.

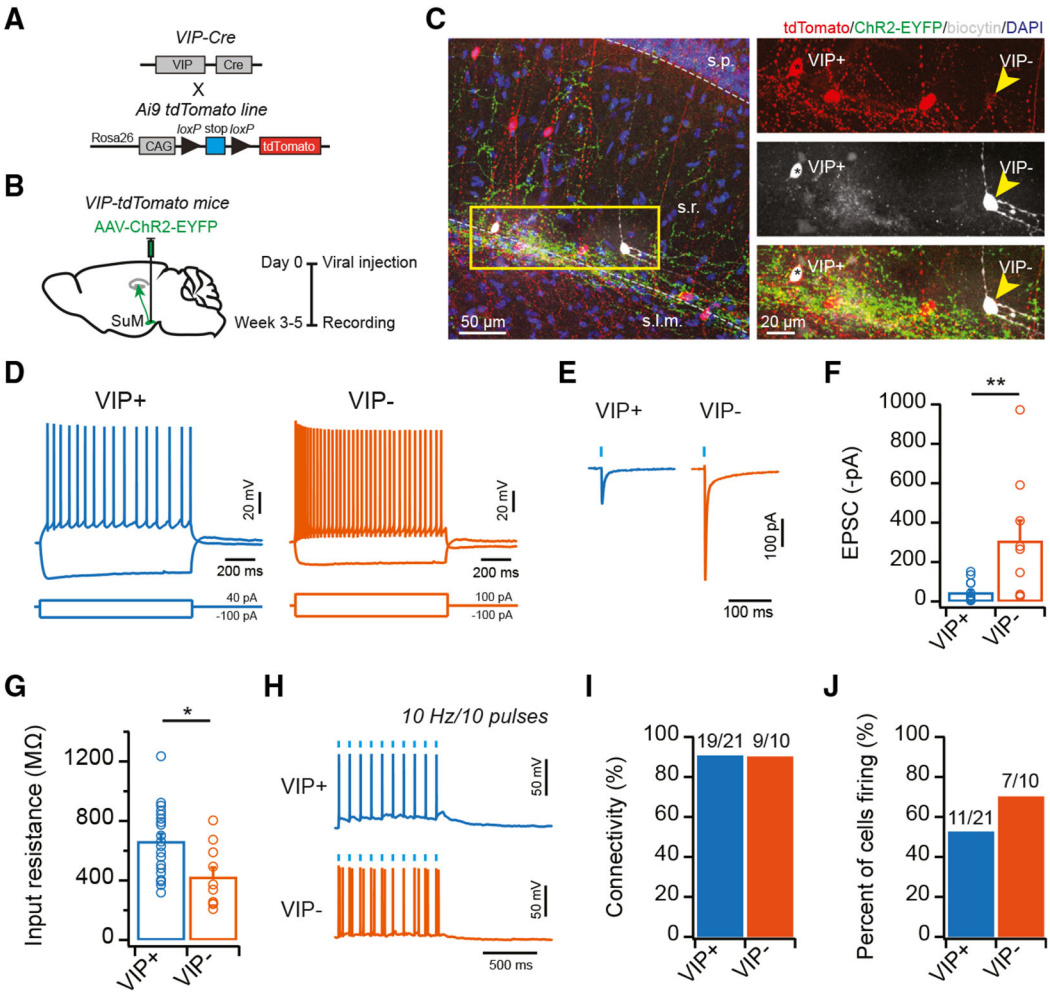

Figure 4. The SuM excites both VIP$^+$ and VIP$^-$ cells in the CA1 SR/SLM border

(A) Genetic strategy to target tdTomato into VIP$^+$ cells by crossing a VIP-IRES-Cre line with a floxed tdTomato reporter line (Ai9).

(B) Experimental procedure and timeline.

(C) Left, a representative confocal image shows a hippocampal slice from a VIP-td mouse that was injected with AAV-ChR2-EYFP into the SuM and underwent whole-cell recording. Right, expanded views of two biocytin-filled VIP$^+$ (asterisk) and VIP$^-$ (arrowhead) cells in the CA1 SR/SLM border.

(D) Current-clamp recording shows the membrane voltage responses to 1 s somatic injections of indicated currents from VIP$^+$ (left) and VIP$^-$ (right) cells.

(E) Voltage-clamp recording shows sample light-evoked EPSC traces recorded from VIP$^+$ and VIP$^-$ cells (holding potential −70 mV). Blue bars represent light pulses.

(F) Group data of light-evoked EPSCs from VIP$^+$ (n = 19 cells/5 mice) and VIP$^-$ cells (n = 9 cells/4mice). **p < 0.01, unpaired t test. Error bars show SEM.

(G) Group data of input resistance from VIP$^+$ (n = 20 cells/5 mice) and VIP$^-$ cells (n = 10 cells/4 mice). *p < 0.05, unpaired t test. Error bars show SEM.

(H) Sample traces of APs evoked by a train of 10 Hz light stimulation in VIP$^+$ (top) and VIP$^-$ (bottom) cells.

(I) Group data of the percentage of VIP^+ and VIP^- cells that receive light-evoked excitatory responses fromthe SuM. The numbers of cells are shown above the bars.
(J) Group data of the percentage of VIP^+ and VIP^- cells that fire APs in response to light stimulation. The numbers of cells are shown above the bars.

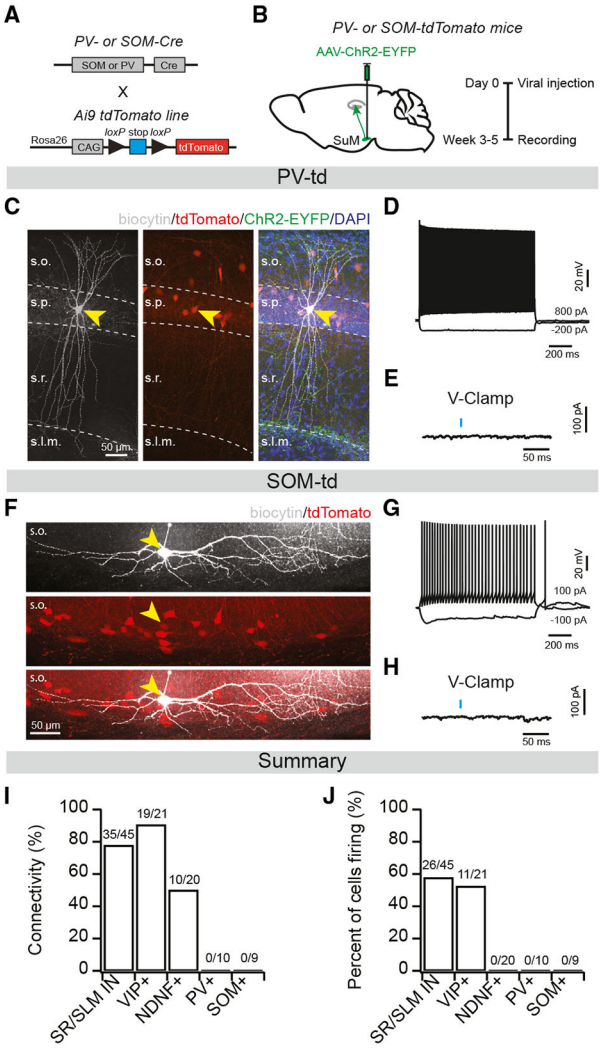

Figure 5. The SuM does not make monosynaptic connections with PV$^+$ or SOM$^+$ cells in CA1

(A) Genetic strategy to target tdTomato into PV$^+$ or SOM$^+$ cells by crossing the PV-IRES-Cre or SOM-IRES-Cre lines with a floxed tdTomato reporter line (Ai9).

(B) Experimental procedure and timeline.

(C) Representative confocal images show a biocytin-filled PV$^+$ cell from a PV-td mouse that underwent whole-cell recording. Arrowhead shows co-labeling of biocytin and tdTomato.

(D) Current-clamp recording shows the membrane voltage responses to 1 s somatic injections of the indicated currents from a PV$^+$ cell. Note the characteristics of the fast-spiking firing pattern of PV$^+$ cells.

(E) Voltage-clamp recording shows no light-evoked excitatory synaptic response in a PV$^+$ cell (holding potential −70 mV).

(F) Representative confocal images show a biocytin-filled SOM$^+$ cell from a SOM-td mouse that underwent whole-cell recording. Arrowhead shows co-labeling of biocytin and tdTomato.

(G) Current-clamp recording shows the membrane voltage responses to 1 s somatic injections of the indicated currents from a SOM$^+$ cell.

(H) Voltage-clamp recording shows no light-evoked excitatory synaptic response in a SOM^+ cell (holding potential −70 mV).
(I) Summary data of the connectivity probability of different subtypes of CA1 interneurons. The numbers of cells are shown above the bars.
(J) Summary data of the percentage of different subtypes of CA1 interneurons that fire APs in response to light stimulation. The numbers of cells are shown above the bars.

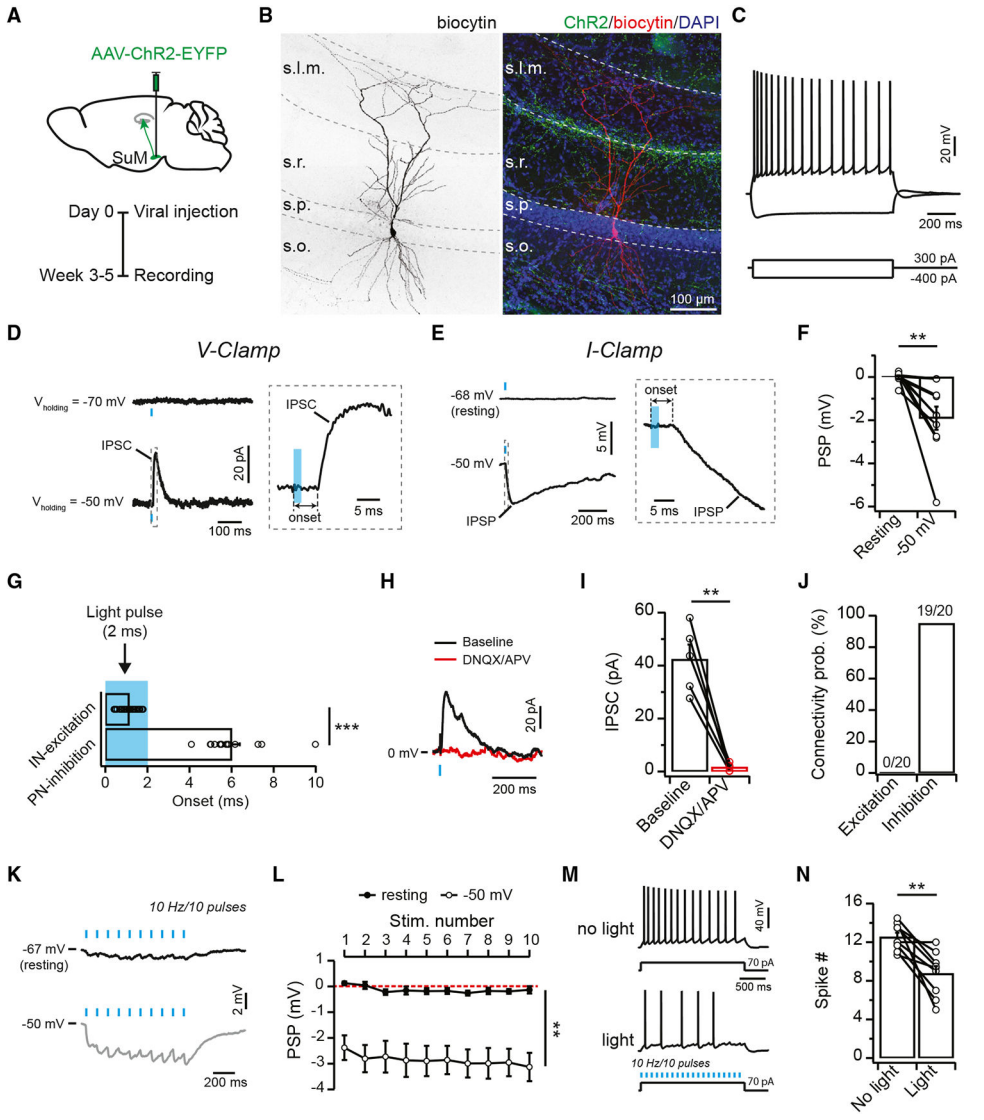

Figure 6. SuM activation drives disynaptic feedforward inhibition to suppress CA1 PN activity

(A) Experimental procedure and timeline.

(B) Sample confocal images show a biocytin-filled CA1 PN that underwent whole-cell recording.

(C) Current-clamp recording shows membrane voltage responses to 1 s depolarizing or hyperpolarizing current injections in a CA1 PN.

(D) Voltage-clamp recording shows the absence of a light-evoked EPSC (top left, holding potential −70 mV) and presence of a light-evoked IPSC (bottom left, holding potential −50 mV) recorded from a CA1 PN. Right: expanded view of the light-evoked IPSC indicated in the bottom left. Note the long delay of onset of the light-evoked IPSC. Blue bars represent light pulses.

(E) Current-clamp recording shows the absence (top left, at resting potential) and presence of a light-evoked PSP (bottom left, at −50 mV) recorded from a CA1 PN. Right: expanded view of the light-evoked PSP indicated in the bottom left. Note the long delay of the onset of light-evoked PSP. Blue bars represent light pulses.

(F) Group data of light-evoked PSPs from individual CA1 PNs at resting potential and −50 mV; $n = 11$ cells/7 mice. $^{**}p < 0.01$, paired t test. Error bars show SEM.
(G) Group data of onset of excitatory synaptic events in SR/SLM interneurons (IN-excitation, $n = 35$ cells/9 mice) versus inhibitory synaptic events in CA1 PNs (PN-inhibition, $n = 14$ cells/7 mice). Blue bar depicts the duration of light pulses. $^{***}p < 0.001$, unpaired t test. Error bars show SEM.
(H and I) Sample traces (H) and group data (I) of light-evoked IPSCs in the absence and presence of DNQX/APV (holding potential 0 mV). $^{**}p < 0.01$, paired t test, $n = 5$ cells/3 mice. Error bars show SEM.
(J) The probability of excitatory and inhibitory connections in CA1 PNs. Numbers of cells are shown above bars.
(K and L) Sample traces (K) and group data (L) of membrane voltage responses evoked by a train of 10 Hz light stimulation at resting potential ($n = 6$ cells/4 mice) or at −50 mV ($n = 8$ cells/4 mice) in CA1 PNs. $^{**}p < 0.01$, two-way ANOVA repeated measures followed by a Tukey test. Error bars show SEM.
(M) Sample traces of spikes elicited by constant current injections, paired without (top) or with (bottom) a train of 10 Hz light stimulation in a CA1 PN.
(N) Group data of the number of spikes elicited by constant current injections, paired without or with a train of 10 Hz light stimulation in CA1 PNs ($n = 9$ cells/5 mice). $^{**}p < 0.01$, paired t test. Error bars show SEM.

KEY RESOURCES TABLE

REAGENT or RESOURCE	SOURCE	IDENTIFIER
Antibodies		
Chicken anti-GFP	Aves lab	Cat #: GFP-1020; RRID:AB_10000240
Goat anti-chicken 488	Thermo Fisher Scientific	Cat #: A11039; RRID:AB_2534096
Streptavidin, Alexa Fluor 594 conjugate	Thermo Fisher Scientific	Cat #: S32356
Streptavidin, Alexa Fluor 647 conjugate	Thermo Fisher Scientific	Cat #: S32357
Bacterial and virus strains		
AAV8-hSyn-ChR2-EYFP	Salk Viral Vector Core	Addgene: #26973
AAVretro-EF1α-mCherry-IRES-Cre	Fenno et al.[57]	Addgene: #55632-AAVrg
AAVdj-EF1A-DIO-hChR2-EYFP-WPRE-pA	Salk Viral Vector Core	Addgene: #20298
rAAV2-hsyn-hChR2(H134R)-EYFP-WPRE-PA	UNC Viral Core	Addgene: #26973
Chemicals, peptides, and recombinant proteins		
Tetrodotoxin (TTX)	Hello Bio	Cat#: HB1035
4-aminopyridine (4-AP)	Hello Bio	Cat#: HB1073
DNQX	Hello Bio	Cat#: HB0262
DL-AP5	Hello Bio	Cat#: HB0251
Biocytin	Hello Bio	Cat#: HB5035
Experimental models: Organisms/strains		
VIP-IRES-Cre	Jackson Laboratory	JAX: 031628
SOM-IRES-Cre	Jackson Laboratory	JAX: 028864
PV-IRES-Cre	Jackson Laboratory	JAX: 017320
NDNF-IRES-Cre	Jackson Laboratory	JAX: 030757
Ai9	Jackson Laboratory	JAX: 007909
Software and algorithms		
pClamp 11	Molecular Devices	N/A
AxoGraph X	AxoGraph	N/A
ImageJ (Fiji)	NIH	N/A
OriginPro 2022	OriginLab	N/A